Available online at www.sciencedirect.com

ScienceDirect

IFAC Papers Online CONFERENCE PAPER ARCHIVE

IFAC-PapersOnLine 48-1 (2015) 802–807

Multi-Variable Integral Sliding Mode Control of a Two Degrees of Freedom Helicopter

Saif S. Butt *, **Harald Aschemann** *

* *Chair of Mechatronics, University of Rostock, D-18059 Rostock, Germany (e-mail: {Saif.Butt, Harald.Aschemann}@uni-rostock.de)*

Abstract: In this paper, a multi-variable nonlinear control-oriented model of a twin rotor aerodynamic system (TRAS) is presented. The mathematical description of the multibody system is derived using Lagrange's equations. Based on the resulting state-space representation, a multi-variable integral sliding mode control is designed to accurately track desired trajectories for both the azimuth angle and the pitch angle. Due to unmeasurable states and uncertainties stemming from simplifications at modelling as well as disturbance torques, a discrete-time extended Kalman filter (EKF) is employed and combined with a discrete-time implementation of the nonlinear control law. The proposed control strategy allows for an excellent tracking behaviour as highlighted by experimental results.

Keywords: Multivariable systems, helicopter control, sliding mode control, extended Kalman filter

1. INTRODUCTION

In this paper, a twin rotor aerodynamic system (TRAS) with two degrees of freedom (DOFs) is considered, which was developed by INTECO (2013), Poland, for control experiments. The first DOF characterises the horizontal rotation of the frame using the azimuth angle, whereas the second one is given by the pitch angle describing the inclination of the frame. In a real helicopter, the aerodynamic force is adjusted by changing the angle of attack. The TRAS, however, uses a changing angular velocity of the propeller for this purpose.

The 2-DOF helicopter system imposes challenging control problems due to its given nonlinearities as well as significant couplings between the pitch axis and the azimuth axis. Moreover, not all state variables are measurable. To achieve a satisfactory tracking performance regarding desired trajectories for the azimuth angle and the pitch angle, a model-based control approach is chosen.

In several contributions, both modelling and experimental identification of similar 2-DOF helicopters set-ups have been investigated,see Ahmad et al. (2000b); Rahideh and Shaheed (2007); Ahmad et al. (2000a); Darus et al. (2004); Shaheed (2004). The methods proposed therein correspond to typical experimental set-ups from different manufacturers, various model-based approaches and methods employing artificial intelligence, e.g., radial basis functions, neural networks and genetic algorithms. In Rahideh and Shaheed (2007), a complete mathematical description of a 2-DOF helicopter using different approaches is described. Regarding the control of the TRAS, a simulation study of a nonlinear predictive control is presented for a ninth-order model in Dutka et al. (2003). In Lopez-Martinez et al. (2004), a feedback-linearising control scheme is proposed for the pitch motion only. Therein, the yaw angle is not considered as a DOF. An H_∞ controller for helicopter dynamics is described in Lopez-Martinez et al. (2003, 2005). The resulting controller exhibits the attributes of a nonlinear PID with time-varying constants according to the operating point. In Ahmed et al. (2009), a sliding mode control dealing with the couplings of a helicopter with two rotors is considered. An adaptive second order sliding mode control has been proposed in Mondal and Mahanta (2012); however, no experimental validation is presented therein. In Butt et al. (2014), a fourth-order nonlinear control-oriented model of a TRAS manufactured by INTECO along with a multi-variable flatness-based control scheme is proposed for a 2-DOF helicopter. In this paper, the same model of the TRAS is employed, and an integral sliding mode control scheme is designed and validated by experiments.

The given paper is structured as follows: In Section 2, a nonlinear control-oriented model of the TRAS is derived according to Butt et al. (2014). A multi-variable integral sliding mode control is proposed in Section 3. The controller is extended by a discrete-time Extended Kalman Filter (EKF) for the estimation of unmeasured states and disturbance torques in Section 4. The discrete-time implementation of both the control law and the EKF are presented in Section 5. In Section 6, experimental results are given that show the performance of the tracking controller as well as the estimator. Finally, conclusions are given in Section 7.

2. CONTROL-ORIENTED MODELING

The TRAS manufactured by INTECO is shown in Fig. 1. It consists of a beam with two propellers – the main and the tail propeller – at both ends of the beam, driven by DC motors. The beam is pivoted in a cardanic joint and can

2405-8963
Peer review under responsibility of International Federation of Automatic Control.
10.1016/j.ifacol.2015.05.129

rotate freely both in the horizontal and vertical planes. Two counterbalance levers with a weight at their ends are fixed to the beam at the pivot. The counterweights determine the steady-state pitch angle without propeller actuation. Two velocity sensors are coupled with the PWM-driven DC motors for the main and tail rotors. The TRAS has two encoders, mounted at the pivot of the azimuth and pitch axes. The multibody system model

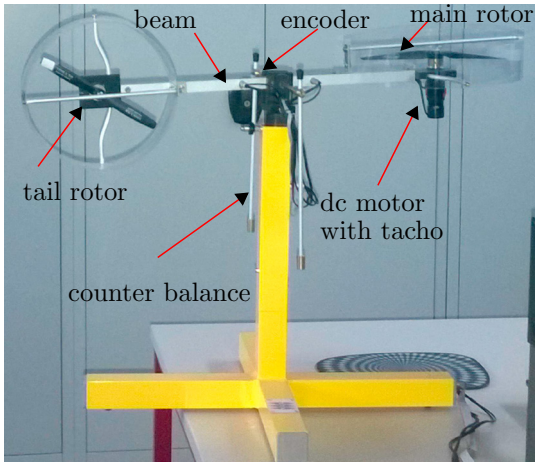

Fig. 1. TRAS test-rig at the Chair of Mechatronics.

for the TRAS consist of the beam, point masses for the two rotors and point masses for the counterbalances. The modelling starts with assigning a right-hand coordinate system with the origin O located at the pivot point of the beam as shown in Fig. 2.

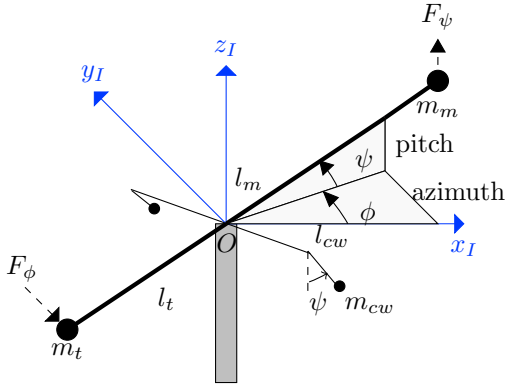

Fig. 2. Free body diagram of TRAS.

The distances of the main rotor and the tail rotor from the origin O are given by l_m and l_t, respectively. The generalized coordinates ϕ and ψ denote the azimuth angle and the pitch angle. Moreover, l_{cw} represents the relevant length of the two levers with the counterweights as point masses m_{cw} at their end. Using a vector notation, the corresponding position vectors $\underline{r}_m$ and $\underline{r}_t$ for the main rotor and the tail rotor, respectively, are given by

$$\underline{r}_m = \begin{bmatrix} l_m \cos\psi \cos\phi \\ l_m \cos\psi \sin\phi \\ l_m \sin\psi \end{bmatrix}, \quad \underline{r}_t = \begin{bmatrix} l_t \cos\psi \cos\phi \\ l_t \cos\psi \sin\phi \\ -l_t \sin\psi \end{bmatrix}. \tag{1}$$

Likewise, the position vectors $\underline{r}_{cw1}$ and $\underline{r}_{cw2}$ for the counterweights at both ends of the beam become

$$\underline{r}_{cw1} = \begin{bmatrix} -l_{cw} \sin\psi \sin\phi \\ -l_{cw} \sin\psi \cos\phi \\ -l_{cw} \cos\psi \end{bmatrix}, \; \underline{r}_{cw2} = \begin{bmatrix} l_{cw} \sin\psi \sin\phi \\ l_{cw} \sin\psi \cos\phi \\ -l_{cw} \cos\psi \end{bmatrix}. \tag{2}$$

The overall kinetic energy of the TRAS is determined with the help of velocity vectors as time derivatives of the corresponding position vectors. The kinetic energy T in terms of the generalized coordinates can be expressed as

$$T = \frac{1}{2}\Big((m_m l_m^2 + m_t l_t^2)(\dot\phi^2 \cos^2\psi + \dot\psi^2) + m_{cw} l_{cw}^2 (\dot\phi^2 \sin^2\psi + \dot\psi^2) + J_z \dot\phi^2 + J_x \dot\psi^2 \Big), \tag{3}$$

where m_m, m_t and m_{cw} represent the point masses at the main rotor, the tail rotor and at the end of the counterweight levers, respectively. The parameters J_z and J_x are the moments of inertia of the rotating beam w.r.t. its body-fixed z-axis and x-axis, respectively. Similarly, the overall potential energy of the point mass system is given as

$$U = \underbrace{\frac{1}{2} k_\phi \phi^2}_{U_\phi} + g\Big((m_m l_m - m_t l_t) \sin\psi + 2 m_{cw} l_{cw} (1 - \cos\psi) \Big). \tag{4}$$

Here, g represents the gravitational acceleration. The restoring energy due to the cable is considered by U_ϕ. The Lagrangian for the system is defined as the difference between the kinetic energy and the potential energy, i.e.,

$$L = T - U. \tag{5}$$

Finally, Lagrange's equations in the presence of non-conservative forces result in

$$\frac{d}{dt}\left(\frac{\partial L}{\partial \dot q}\right) - \frac{\partial L}{\partial q} = \tau_q - \frac{\partial R}{\partial \dot q}, \quad q = \{\phi, \psi\} \tag{6}$$

where τ_ψ and τ_ϕ are net torques along the pitch and the azimuth axes. The Rayleigh function R is given by

$$R = \frac{1}{2} c_\phi \dot\phi^2 + \frac{1}{2} c_\psi \dot\psi^2 . \tag{7}$$

Substituting Eq. (3), Eq. (4) and Eq. (5) into Eq. (6), the equations of motion for the system result in

$$J_\phi \ddot\phi = \tau_\phi + J \dot\phi \dot\psi \sin(2\psi) - k_\phi \phi - c_\phi \dot\phi, \tag{8}$$

$$J_\psi \ddot\psi = \tau_\psi - J \frac{\dot\phi^2}{2} \sin(2\psi) - c_\psi \dot\psi - g\Big((m_m l_m - m_t l_t) \cos\psi + 2 m_{cw} l_{cw} \sin\psi \Big), \tag{9}$$

with

$$J_\phi = (m_m l_m^2 + m_t l_t^2) \cos^2\psi + 2 m_{cw} l_{cw}^2 \sin^2\psi + J_z, \tag{10}$$

$$J_\psi = m_m l_m^2 + m_t l_t^2 + 2 m_{cw} l_{cw}^2 + J_x, \tag{11}$$

$$J = m_m l_m^2 + m_t l_t^2 - 2 m_{cw} l_{cw}^2. \tag{12}$$

It can be seen that the differential equations with respect to the pitch angle and the azimuth angle are highly nonlinear and contain coupling terms. The net torques acting along the azimuth and the pitch axes are given by

$$\tau_\phi = F_\phi l_t \cos\psi , \tag{13}$$

$$\tau_\psi = F_\psi l_m . \tag{14}$$

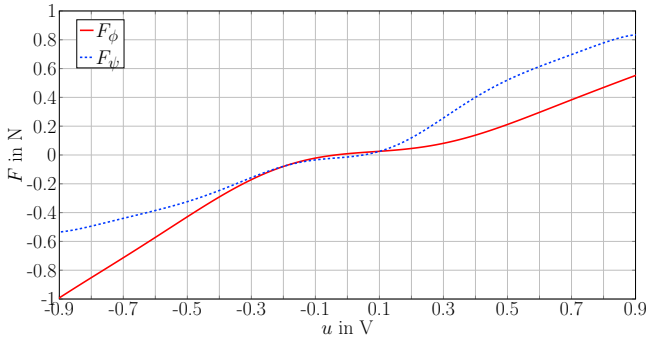

Fig. 3. Thrust characteristics as a function of the PWM voltage.

The relationship between the propulsive forces F_ϕ and F_ψ and the PWM input voltages u_t and u_m for the tail rotor and the main rotor, respectively, is identified experimentally, see Fig. 3. An inverse map of the nonlinear characteristic curve is implemented with the help of a lookup table that transforms the propulsive forces into corresponding PWM inputs.

To handle the parametric uncertainties and unknown disturbances, the model is extended with two lumped disturbance torques z_ϕ and z_ψ acting on the azimuth and pitch axes, respectively. Hence, the extended nonlinear state-space model can be written as

$$\underbrace{\begin{bmatrix}\dot\phi\\ \ddot\phi\\ \dot\psi\\ \ddot\psi\end{bmatrix}}_{\dot{\underline{x}}} = \underbrace{\begin{bmatrix} \dot\phi \\ \frac{1}{J_\phi}\Big(-(c_\phi\dot\phi + k_\phi\phi) + J\dot\phi\dot\psi\sin(2\psi) + z_\phi\Big) \\ \dot\psi \\ \frac{1}{J_\psi}\Big(-(c_\psi\dot\psi + k_\psi\psi) - J\frac{\dot\phi^2}{2}\sin(2\psi) + z_\psi - \\ g\big((m_m l_m - m_t l_t)\cos\psi + 2m_{cw}l_{cw}\sin\psi\big)\Big)\end{bmatrix}}_{\underline{f}(\underline{x})} + \underbrace{\begin{bmatrix} 0 & 0 \\ \frac{l_t\cos(\psi)}{J_\phi} & 0 \\ 0 & 0 \\ 0 & \frac{l_m}{J_\psi}\end{bmatrix}}_{\underline{B}(\underline{x})} \underbrace{\begin{bmatrix}F_\phi\\ F_\psi\end{bmatrix}}_{\underline{u}}. \tag{15}$$

These disturbance torques account for parametric uncertainty, unmodelled dynamics and all disturbances affecting the system. Among these are non-modelled effects due to the supply cables and gyroscopic torques as well as the couplings caused by the tail rotor and the main rotor in the case of angular accelerations of the propellers.

The output vector $\underline{y}$ is identical to the measurement vector $\underline{y}_m$ and contains both generalized coordinates

$$\underline{y}(t) = \underline{y}_m(t) = [\,\phi\ \psi\,]^T. \tag{16}$$

3. INTEGRAL SLIDING MODE CONTROL

In the case of parameter uncertainties, flatness-based control schemes with linear stabilizing control laws are prone to robustness issues. Therefore, an integral sliding mode control (I-SMC) is proposed in this paper. The aim of a sliding mode controller is to drive the state trajectory towards a sliding surface in the state space and to maintain the state trajectory on this surface afterwards, cf. Slotine and Li (1991); Young et al. (1999). The sliding surface is independent of the disturbances and parameter variations and, as a result, overcomes robustness issues. Let e_ϕ and e_ψ denote the errors between the measured and the desired trajectories (denoted with a subscript d) for the azimuth angle and the pitch angle according to

$$e_\phi = \phi - \phi_d \quad \text{and} \quad e_\psi = \psi - \psi_d. \tag{17}$$

Accurate tracking of desired trajectories for the azimuth angle and the pitch angle can be achieved by the following choice of the sliding surfaces

$$\underline{s}(\underline{x}) = \begin{bmatrix} s_\phi(\underline{x}) \\ s_\psi(\underline{x})\end{bmatrix}, \tag{18}$$

with

$$s_i(\underline{x}) = \dot e_i + \alpha_{i1}e_i + \alpha_{i0}\int_0^t e_i\ \mathrm{d}\tau\ , \quad i \in [\phi,\psi]\ . \tag{19}$$

Here, the integral actions are introduced to avoid steady-state errors. The integral sliding mode control can be divided into two phases: the sliding phase with $\underline{s}(\underline{x}) = \underline{0}, \dot{\underline{s}}(\underline{x}) = \underline{0}$, and the reaching phase with $\underline{s}(\underline{x}) \neq \underline{0}$. The control input during the ideal sliding mode represents the equivalent control $\underline{u}_{eq} = [u_{eq,\phi}, u_{eq,\psi}]^T$, whereas an additional switching control action $\underline{u}_{sw} = [u_{sw,\phi}, u_{sw,\psi}]^T$ provides a finite-time convergence to the sliding surfaces during the reaching phase. Subsequently, the overall control input u_i can be expressed as the sum of both terms

$$u_i = u_{eq,i} + u_{sw,i}\ . \tag{20}$$

The differentiation of the sliding surfaces s_ϕ and s_ψ with respect to time results in

$$\dot{\underline{s}}(\underline{x}) = \begin{bmatrix} \ddot\phi - \ddot\phi_d + \alpha_{\phi1}(\dot\phi - \dot\phi_d) + \alpha_{\phi0}(\phi - \phi_d) \\ \ddot\psi - \ddot\psi_d + \alpha_{\psi1}(\dot\psi - \dot\psi_d) + \alpha_{\psi0}(\psi - \psi_d)\end{bmatrix}. \tag{21}$$

The sliding condition implies that $\forall t \geq t_1$ the output trajectory remain on the sliding surfaces $\underline{s}(\underline{x}) = \underline{0}$. By choosing strictly positive coefficients of the Hurwitz polynomial, it can be ensured that the closed-loop system is asymptotically stable during the ideal sliding mode. In this case, the error dynamics is governed by

$$\ddot e_i + \alpha_{i1}\dot e_i + \alpha_{i0}e_i = 0\ , \quad i \in [\phi,\psi]\ , \tag{22}$$

where the strictly positive coefficients $\alpha_{i1} > 0$ and $\alpha_{i0} > 0$ denote coefficient of Hurwitz polynomials. Substituting $\ddot\phi$ and $\ddot\psi$ from Eq. (15) into Eq. (21), and solving for the equivalent control vector $\underline{u}_{eq}$ results in the following expressions

$$u_{eq,\phi} = -\frac{J_\phi\nu_1 - (c_\phi\dot\phi + k_\phi\phi) + J\dot\phi\dot\psi\sin(2\psi) + z_\phi}{l_t\cos\psi}\ , \tag{23}$$

$$u_{eq,\psi} = -\frac{1}{l_m}\Big(J_\psi\nu_2 - (c_\psi\dot\psi + k_\psi\psi) - J\frac{\dot\phi^2}{2}\sin(2\psi) + z_\psi - g(m_m l_m - m_t l_t)\cos\psi - 2gm_{cw}l_{cw}\sin\psi\Big)\ , \tag{24}$$

with

$$\begin{bmatrix}\nu_1\\ \nu_2\end{bmatrix} = \begin{bmatrix} \ddot\phi_d - \alpha_{\phi1}(\dot\phi - \dot\phi_d) - \alpha_{\phi0}(\phi - \phi_d) \\ \ddot\psi_d - \alpha_{\psi1}(\dot\psi - \dot\psi_d) - \alpha_{\psi0}(\psi - \psi_d)\end{bmatrix}. \tag{25}$$

The equivalent control input corresponds to the ideal motion of the system on the sliding surfaces $\underline{s}(\underline{x}) = \underline{0}$.

However, when the initial state is not located on the sliding surfaces, an additional switching control part to be designed in the next step brings the state back to the sliding surfaces – the reaching phase – and keeps it on the surfaces $\underline{s}(\underline{x}) = \underline{0}$ despite disturbances and uncertainties. Considering a quadratic Lyapunov $V(\underline{x})$ function of the form

$$V(\underline{x}) = \frac{1}{2}\underline{s}(\underline{x})^T\underline{s}(\underline{x}) = \frac{1}{2}s_\phi^2 + \frac{1}{2}s_\psi^2 \ , \tag{26}$$

the control input vector $\underline{u}_{sw}$ must be chosen in such a way that the time derivative

$$\dot{V}(\underline{x}) = s_\phi\dot{s}_\phi + s_\psi\dot{s}_\psi \leq -\eta_\phi|s_\phi| - \eta_\psi|s_\psi| < 0 \tag{27}$$

is negative definite. Substituting Eq. (20) and Eq. (24) into Eq. (21) and solving for the switching control input $\underline{u}_{sw}$ leads to

$$\dot{V}(\underline{x}) = s_\phi \underbrace{\frac{l_t\cos(\psi)}{J_\phi}u_{sw,\phi}}_{-\eta_\phi\,\mathrm{sgn}(s_\phi)} + s_\psi \underbrace{\frac{l_m}{J_\psi}u_{sw,\psi}}_{-\eta_\psi\,\mathrm{sgn}(s_\psi)} < 0 \ . \tag{28}$$

The parameters $\eta_\phi > 0$ and $\eta_\psi > 0$ determine the switching heights and guarantee that the Lyapunov function becomes negative definite.

The integral sliding mode control presented so far is subject to the chattering phenomenon. This involves fast switching actions introduced by the sgn function, and may lead to the excitation of unmodelled high-frequency dynamics. To counteract this effect, smooth switching functions $\tanh(s_i/\epsilon)$ with a strictly positive constant $\epsilon > 0$ – influencing a boundary layer thickness – are utilized. The chattering reduction depends on value of ϵ at the cost of robustness. The larger the value of ϵ, the more the chattering phenomenon is suppressed. At the same time, however, the robustness will be reduced and the ideal sliding mode becomes a real sliding mode with corresponding tracking errors.

The control laws are implemented in a discrete-time form with a small sampling time of $T_s = 1$ ms. The control design, hence, represents a quasi-continuous one.

4. DISCRETE-TIME EXTENDED KALMAN FILTER

To estimate the angular velocities as well as the lumped disturbance torques, a discrete-time extended Kalman filter (EKF) is employed. For this purpose, integrator disturbance models are introduced according to

$$\dot{z}_\phi = 0, \quad \text{and} \quad \dot{z}_\psi = 0. \tag{29}$$

Note that these disturbance models are excited in the case of output errors between the measured and the estimated output variables. The state vector of the extended system representation results in

$$\underline{x}_e = \left[\ \phi\ \dot{\phi}\ \psi\ \dot{\psi}\ z_\phi\ z_\psi\ \right]^T \ , \tag{30}$$

and the measurement vector becomes

$$\underline{y}_m = \underline{C}_{m,e}\,\underline{x}_e = \begin{bmatrix} 1&0&0&0&0&0 \\ 0&0&1&0&0&0 \end{bmatrix}\underline{x}_e \ . \tag{31}$$

Given the continuous-time state equation of the extended system

$$\dot{\underline{x}}_e = \underline{f}(\underline{x}_e, \underline{u}), \tag{32}$$

an explicit Euler time-discretization of Eqs. (32) as well as an introduction of additive noise processes lead to the following discrete-time state-space representation used for the EKF design

$$\underline{x}_{e,k+1} = \underbrace{\underline{x}_{e,k} + T_s\underline{f}_k(\underline{x}_{e,k}, \underline{u}_k)}_{\underline{\varphi}_k(\underline{x}_{e,k},\underline{u}_k)} + \underline{w} \ , \tag{33}$$

$$\underline{y}_{m,k} = \underline{C}_{m,e}\underline{x}_{e,k} + \underline{v}. \tag{34}$$

Here, T_s denotes the sampling time, $\underline{x}_{e,k}$ the extended state vector, $\underline{u}_k$ the control input vector, and $\underline{y}_{m,k}$ the measured output at discrete-time t_k. Furthermore, the process noise and the measurement noise are given by $\underline{w}$ and $\underline{v}$, respectively. Both are assumed to be zero-mean Gaussian white noise processes with zero cross-correlation. The vanishing cross-correlation leads to diagonal covariance matrices $\underline{Q}$ and $\underline{R}$ characterising the process noise $\underline{w}$ and the measurement noise $\underline{v}$, respectively. Fig. 4 shows that the discrete-time EKF implementation can be divided into two stages, namely a prediction stage and an innovation stage Stengel (1994). The error covariance matrix is

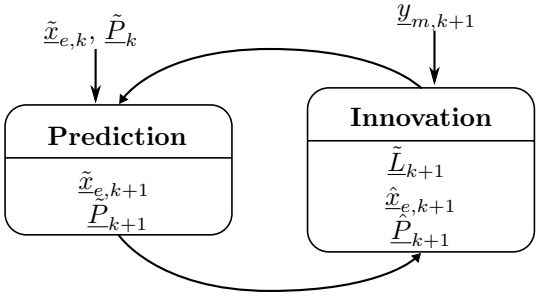

Fig. 4. Implementation of the discrete-time EKF.

denoted by $\underline{P}_k$. The algorithm for the discrete-time EKF can be summarized at each time t_k as follows, cf. Stengel (1994):

- State prediction

$$\tilde{\underline{x}}_{e,k+1} = \underline{\varphi}_k(\hat{\underline{x}}_{e,k}, \underline{u}_k) \tag{35}$$

- Prediction of the error covariance matrix $\tilde{\underline{P}}_{k+1}$

$$\tilde{\underline{P}}_{k+1} = \underline{\Phi}_k\hat{\underline{P}}_k\underline{\Phi}_k^T + \underline{Q} \ , \text{ with } \underline{\Phi}_k = \frac{\partial\underline{\varphi}(\hat{\underline{x}}_{e,k}, \underline{u}_k)}{\partial\underline{x}_{e,k}}\Big|_{\hat{\underline{x}}_{e,k}} \tag{36}$$

- Update of the gain matrix $\tilde{\underline{L}}_{k+1}$

$$\tilde{\underline{L}}_{k+1} = \tilde{\underline{P}}_{k+1}\underline{C}_{m,e}^T\big(\underline{C}_{m,e}\tilde{\underline{P}}_{k+1}\underline{C}_{m,e}^T + \underline{R}\big)^{-1} \tag{37}$$

- Update of the state vector $\hat{\underline{x}}_{e,k+1}$

$$\hat{\underline{x}}_{e,k+1} = \tilde{\underline{x}}_{e,k+1} + \tilde{\underline{L}}_{k+1}\big(\underline{y}_{m,k+1} - \underline{C}_{m,e}\tilde{\underline{x}}_{e,k+1}\big) \tag{38}$$

- Update of the error covariance matrix for the next sampling interval

$$\hat{\underline{P}}_{k+1} = \big(\underline{I} - \tilde{\underline{L}}_{k+1}\underline{C}_{m,e}\big)\tilde{\underline{P}}_{k+1} \tag{39}$$

The closed-loop stability of the overall control structure consisting of the multi-variable integral sliding mode control and the discrete-time EKF has been investigated thoroughly by simulations.

5. IMPLEMENTATION OF THE CONTROL STRUCTURE

The time-discrete implementation scheme of the multi-variable integral sliding mode control combined with a

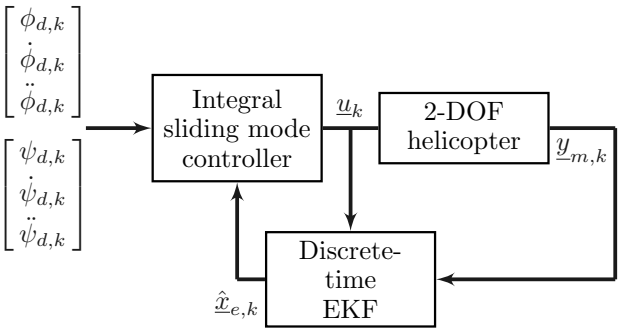

Fig. 5. Control implementation.

discrete-time EKF is shown in Fig. 5.
The TRAS is equipped with a dedicated I/O board and a power interface. The control computer communicates with the incremental sensors and motors interfaced by means of the dedicated I/O board. The I/O board is operated by a real-time software within the MATLAB/Simulink environment.

6. EXPERIMENTAL RESULTS

The parameter values for the spring and the damping coefficients identified experimentally with the help of a nonlinear least-squares minimization are listed in Table 1.

Table 1. Parameters of the TRAS

Parameter	Value	Units
c_ψ	0.095	Nm · s
c_ϕ	0.008	Nm · s
k_ϕ	0.060	Nm

The counterweights have been adjusted in such a way that the the azimuth angle and the pitch angle lies in the following range:

$$0 \text{ rad} \leq \phi \leq 6.5 \text{ rad}$$
$$0 \text{ rad} \leq \psi \leq 2 \text{ rad}.$$

The covariance matrices $\underline{Q}$, $\underline{R}$ and initial error covariance matrix $\underline{P}_0$ for the discrete-time EKF have been chosen properly to achieve fast error a convergence rate as well as to minimize the effect of measurement and process noise on the estimates. The controller is activated at t = 5 s.
The desired and measured trajectories for the azimuth angle, cf. Fig. 6, are in good agreement during both the transient phase as well as in steady-state.
Subsequently, an excellent trajectory tracking behaviour is obtained for the pitch angle as depicted in Fig. 7.
The corresponding errors in the azimuth angle and the pitch angle are shown in Fig. 8. It can be seen that the maximum steady-state errors are smaller than 0.02 rad for both the azimuth angle and the pitch angle. On the other hand, the maximum absolute error during the transient phase is 0.25 rad and 0.1 rad for the azimuth angle and the pitch angle, respectively. The proposed controller, hence, tracks the desired trajectories well and furthermore, provides steady-state accuracy. The corresponding control inputs for the pitch axis and azimuth axis are shown in Fig. 9.
The angular velocities of the pitch and azimuth axis are

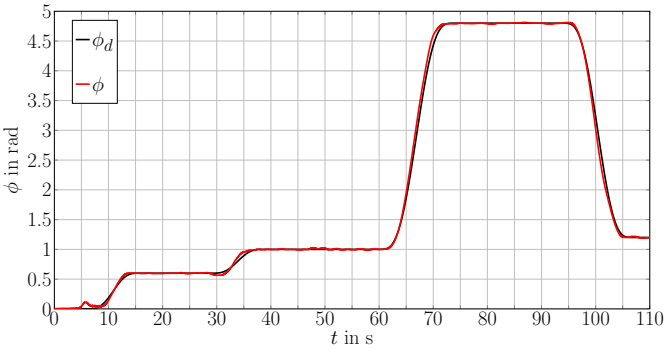

Fig. 6. Trajectory tracking w.r.t. the azimuth angle.

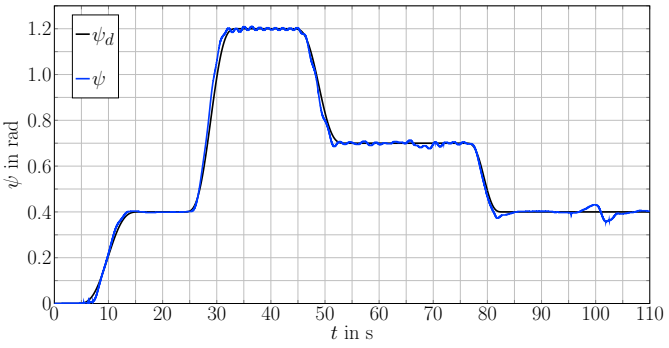

Fig. 7. Trajectory tracking w.r.t. the pitch angle.

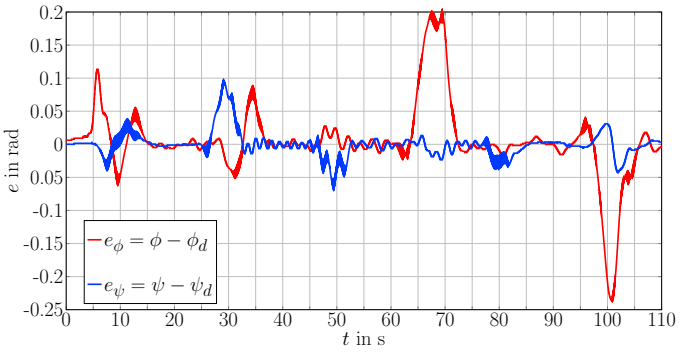

Fig. 8. Tracking error w.r.t. the azimuth angle and the pitch angle.

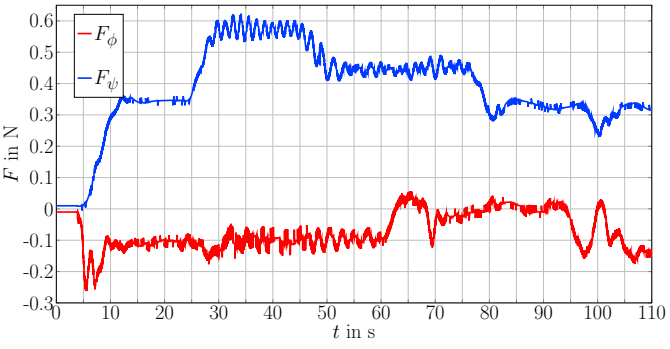

Fig. 9. Control inputs w.r.t. the pitch axis and azimuth axis.

not directly available by measurements. The corresponding estimates of the EKF for the angular velocities are depicted in Fig. 10.
Fig. 11 shows the estimated lumped disturbance torques

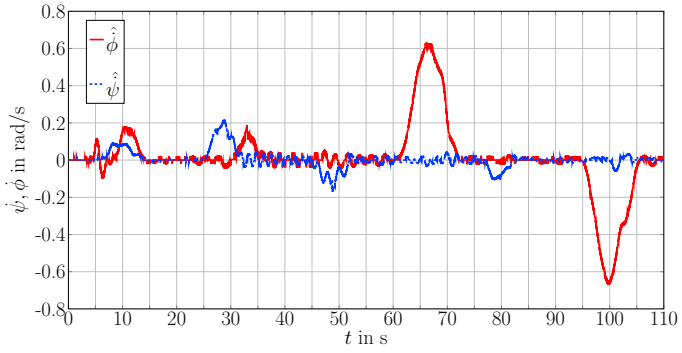

Fig. 10. Estimated angular velocities.

acting on the pitch and azimuth axis. The magnitudes of the estimated disturbance torques show that it is vital to consider them in the control design for an accurate trajectory tracking.

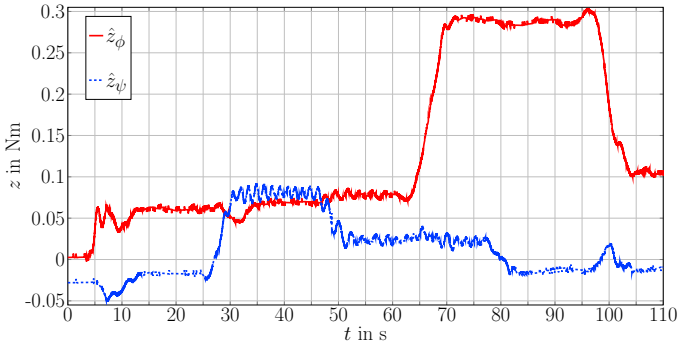

Fig. 11. Estimated disturbance torques.

7. CONCLUSION

In this paper, a nonlinear control-oriented model of a two degree of freedom helicopter is derived. The propulsive forces acting on the main rotor and the tail rotor are chosen as control inputs. A multi-variable integral sliding mode control is proposed to track desired trajectories for the azimuth angle as well as the pitch angle. For the estimation of the unmeasured angular velocities and lumped disturbance torques acting on the 2-DOF helicopter, a discrete-time EKF is employed. Thereby, given process and measurement noise can be addressed properly. Experiment results show that an excellent tracking behaviour with small errors is obtained for both outputs.

REFERENCES

Ahmad, S., Chipperfield, A., and Tokhi, M. (2000a). Dynamic Modeling and Optimal Control of a Twin Rotor MIMO System. In *National Aerospace and Electronics Conf., 2000. NAECON 2000. Proc. of the IEEE 2000*, 391–398.

Ahmad, S., Shaheed, M., Chipperfield, A., and Tokhi, M. (2000b). Nonlinear Modelling of a Twin Rotor MIMO System using Radial Basis Function Networks. In *National Aerospace and Electronics Conf., 2000. NAECON 2000. Proc. of the IEEE 2000*, 313–320.

Ahmed, Q., Bhatti, A., and Iqbal, S. (2009). Nonlinear Robust Decoupling Control Design for Twin Rotor System. In *Asian Control Conf., 2009. ASCC 2009. 7th*, 937–942.

Butt, S.S., Prabel, R., and Aschemann, H. (2014). Multi-Variable Flatness-Based Control of a Two Degrees of Freedom Helicopter. In *Control, Decision and Information Technologies (CoDIT), 2014 International Conf. on*, 321–326.

Darus, I.Z.M., Aldebrez, F., and Tokhi, M. (2004). Parametric Modelling of a Twin Rotor System using Genetic Algorithms. In *Control, Communications and Signal Processing, 2004. First International Symposium on*, 115–118.

Dutka, A., Ordys, A., and Grimble, M. (2003). Non-Linear Predictive Control of 2 DOF Helicopter Model. In *Decision and Control, 2003. Proc. 42nd IEEE Conf. on*, volume 4, 3954–3959 vol.4.

INTECO (2013). Two Rotor Aero-Dynamical System User's Manual.

Lopez-Martinez, M., Diaz, J.M., Ortega, M., and Rubio, F. (2004). Control of a Laboratory Helicopter using Switched 2-Step Feedback Linearization. In *American Control Conf., 2004. Proc. of the 2004*, volume 5, 4330–4335 vol.5.

Lopez-Martinez, M., Ortega, M., and Rubio, F. (2003). An H_∞ Controller for a Double Rotor System. In *Emerging Technologies and Factory Automation, 2003. Proc. ETFA '03. IEEE Conf.*, volume 1, 253–259 vol.1.

Lopez-Martinez, M., Vivas, C., and Ortega, M. (2005). A Multivariable Nonlinear H_∞ Controller for a Laboratory Helicopter. In *Decision and Control, 2005 and 2005 European Control Conf. CDC-ECC '05. 44th IEEE Conf. on*, 4065–4070.

Mondal, S. and Mahanta, C. (2012). Adaptive Second-order Sliding Mode Controller for a Twin Rotor Multi-Input-Multi-Output System. *Control Theory Applications, IET*, 6(14), 2157–2167. doi:10.1049/iet-cta.2011.0478.

Rahideh, A. and Shaheed, M.H. (2007). Mathematical Dynamic Modelling of a Twin-Rotor Multiple Input-Multiple Output System. *Proc. of the Institution of Mechanical Engineers, Part I: Journal of Systems and Control Engineering*, 221(1), 89–101.

Shaheed, M. (2004). Performance Analysis of 4 types of Conjugate Gradient Algorithms in the Nonlinear Dynamic Modelling of a TRMS using Feedforward Neural Networks. In *Systems, Man and Cybernetics, 2004 IEEE International Conf. on*, volume 6, 5985–5990 vol.6.

Slotine, J. and Li, W. (1991). *Applied Nonlinear Control*. Prentice-Hall, Inc.

Stengel, R. (1994). *Optimal Control and Estimation*. Dover Publications, Inc.

Young, K., Utkin, V., and Ozguner, U. (1999). A Control Engineer's Guide to Sliding Mode Control. *Control Systems Technology, IEEE Trans. on*, 7(3), 328–342.